PHYSICAL REVIEW D **92,** 074036 (2015)

Geometrical scaling in inelastic inclusive particle production at the LHC

Michał Praszałowicz and Anna Francuz

M. Smoluchowski Institute of Physics, Jagiellonian University, Łojasiewicza 11, 30-348 Kraków, Poland

(Received 12 August 2015; published 23 October 2015)

Analyzing recent ALICE data on inelastic pp scattering at the LHC energies, we show that charged particle distributions exhibit geometrical scaling (GS). We show also that the inelastic cross section is scaling as well and that in this case the quality of GS is better than for multiplicities. Moreover, exponent λ characterizing the saturation scale is for the cross-section scaling compatible with the one found in deep inelastic ep scattering at HERA. Next, by parametrizing charged particle distributions by the Tsallis-like formula, we find a somewhat unexpected solution that still exhibits GS, but differs from the "standard" one where the Tsallis temperature is proportional to the saturation scale.

DOI: 10.1103/PhysRevD.92.074036 PACS numbers: 13.85.Ni, 12.38.Lg

I. INTRODUCTION

It is believed that gluon distribution inside a hadron saturates at small Bjorken x (see Refs. [1,2] for review). This is a consequence of the nonlinear QCD evolution equations, known as the Balitsky-Kovchegov (BK) equation [3] or in a more general case as the JIMWLK equation [4], that possesses traveling wave solutions [5]. The latter property, in the QCD context, is called geometrical scaling (GS) [6]. An effective theory relevant for the small Bjorken x region is the so-called color glass condensate (CGC) [7]. For the purpose of the present work the details of the saturation are not of primary importance; it is the very existence of the saturation scale, which plays the crucial role.

Geometrical scaling means that some observable N that in principle depends on two independent kinematical variables, say x and Q^2, in fact depends only on a specific combination of them denoted as τ,

$$N(x,Q^2)=\mathcal{F}(\tau). \tag{1}$$

Here function $\mathcal{F}$ in Eq. (1) is a dimensionless function of a scaling variable [8]

$$\tau=Q^2/Q_s^2(x), \tag{2}$$

and

$$Q_s^2(x)=Q_0^2(x/x_0)^{-\lambda} \tag{3}$$

is the saturation scale. The power law form of the saturation scale is dictated by a saddle-point solution to the BK equation and has been tested phenomenologically for different high energy processes [6,9–11].

Here we are coming back to pp scattering [9] in the context of recently published ALICE data [12] for charged particle distributions at three LHC energies 0.9, 2.76, and 7 TeV. After discussing shortly in Sec. II how GS emerges in the k_T factorization scheme, we shall show in Sec. III that recent ALICE data indeed exhibit geometrical scaling with, however, the λ exponent being different than in the case of deep inelastic (DIS) ep scattering. Interestingly, we shall also show that the inclusive cross sections scale somewhat better and with an exponent that is very close to the DIS value $\lambda=0.32$ [10]. This result calls for a better understanding of the impact parameter picture of pp scattering in the context of the saturation physics and the color glass condensate theory.

Another topic addressed in the present paper is the shape of the scaling function introduced schematically in Eq. (1). Function $\mathcal{F}$ can, in fact, be obtained numerically only within some specific model. Here, we shall use phenomenological parametrization in the form of Tsallis-like distribution [13] applied successfully in the past to describe spectra of charged particles [14–16]. In Sec. IV we briefly describe how GS should be reflected in the Tsallis distribution. Next, in Sec. V we shall try to fit Tsallis-like parametrization to the ALICE data. Unfortunately, as already remarked in the original ALICE publication [12], this piece of data does not admit a good quality Tsallis fit. Nevertheless, we invoke a procedure that allows for rather good description of the data in the range of moderate transverse momenta where GS is expected to occur. Somewhat unexpectedly we find a GS scaling solution that is very different from the "standard" one described in Sec. IV. Unfortunately, GS in this solution is rather accidental, and, as will be shown in the end of Sec. V, it will disappear at very high energies. Whether this is only a property of the Tsallis parametrization "forced" to describe ALICE data, or a real prediction, remains to be seen. We conclude in Sec. VI.

II. GEOMETRICAL SCALING IN HADRONIC COLLISIONS

The cross section for producing a gluon with moderate p_T in hadronic collision can be described in the so-called k_T factorization scheme as a scattering of two gluonic systems [17],

$$\frac{d\sigma}{dyd^2p_{\rm T}} = \frac{C}{p_{\rm T}^2}\int d^2\vec{k}_{\rm T}\alpha_{\rm s}(k_{\rm T}^2)\varphi_1(x_1,\vec{k}_{\rm T}^2)\varphi_2(x_2,(\vec{k}-\vec{p})_{\rm T}^2), \tag{4}$$

characterized by the unintegrated gluon distributions $\varphi_{1,2}$. Here C contains color factors and numerical constants. Bjorken x's of colliding gluons read

$$x_{1,2} = \frac{p_{\rm T}}{\sqrt{s}}e^{\pm y}. \tag{5}$$

Formula (4) has been proven in Ref. [18] for the scattering of a dilute system on a dense one. It is, however, commonly conjectured also for dense-dense scattering, which is actually the case we are dealing with here. In the following we are interested in central rapidity production where $y \simeq 0$, i.e., $x_1 \simeq x_2 = x$, and therefore both gluonic distributions $\varphi_{1,2}$ are characterized by one saturation scale. Generalization to the case of $y \neq 0$ is possible, but the GS violation is expected when one of the Bjorken x's becomes too large [11].

There exist many models of unintegrated gluon distributions (see, e.g., [19]); the simplest ones are the Golec-Biernat–Wüsthoff (GBW) model [20] or the one by Kharzeev, Levin, and Nardi [21]. These two models share two important features: geometrical scaling (which is, however, not present in other models of unintegrated gluon distributions; see, e.g., Ref. [22]) and dependence on the transverse area $S_\perp$ whose precise meaning is best understood in a picture where the impact parameter is also taken into account [23,24]. Therefore,

$$\varphi(x,\vec{k}_{\rm T}^2) = S_\perp\phi(k_{\rm T}^2/Q_{\rm s}^2(x)), \tag{6}$$

where ϕ is a dimensionless function of the scaling variable $k_{\rm T}^2/Q_{\rm s}^2(x)$, rather than independently of x and $k_{\rm T}^2$. Of course, geometrical scaling is only an approximation and is expected to break for large Bjorken x's and also for large transverse momenta. We also expect GS breaking for small $k_{\rm T}$ where nonperturbative effects including effects from the pion mass are of importance. Ignoring these effects and neglecting also momentum dependence of the strong coupling constant, we arrive at

$$\left.\frac{d\sigma}{dyd^2p_{\rm T}}\right|_{y=0} = \frac{S_\perp^2}{2\pi}\mathcal{F}(\tau), \tag{7}$$

where $\mathcal{F}$ is a universal, energy independent function of the scaling variable τ,

$$\tau = \frac{p_{\rm T}^2}{Q_{\rm s}^2(x)} = \left(\frac{p_{\rm T}}{Q_0}\right)^2\left(\frac{p_{\rm T}}{\xi W}\right)^\lambda. \tag{8}$$

Here we have used (3) for the saturation scale $Q_{\rm s}^2$. We take for $x_0 = \xi\times 10^{-3}$. This implies that in (8) $p_{\rm T}$ is in GeV/c and W in TeV. Furthermore for Q_0 we can take without any loss of generality $Q_0 = 1$ GeV/c. As already mentioned we are considering here only midrapidity production, and therefore we shall skip in the following subscript $y = 0$.

One typically assumes that $S_\perp$ is an energy independent constant. This is true in the case of the GBW model [20] where $S_\perp = \sigma_0$ with σ_0 characterizing the asymptotics of the dipole-proton cross section for large dipole sizes. In the case of heavy ion collisions for fixed centrality, $S_\perp$ has geometrical interpretation as an overlap area of two colliding nuclei [21]. In this case one can therefore assume that

$$\frac{d\sigma}{dyd^2p_{\rm T}} = S_\perp\frac{d^2N}{dyd^2p_{\rm T}}, \tag{9}$$

where N is a multiplicity of produced gluons. Neglecting possible energy dependence of gluon fragmentation into hadrons [25], i.e., adopting the parton-hadron duality hypothesis [26], we arrive at

$$\frac{1}{p_{\rm T}}\frac{d^2N_{\rm ch}}{dydp_{\rm T}} = S_\perp\mathcal{F}(\tau). \tag{10}$$

Here the "transition factor" that converts the number of gluons to the multiplicity of produced hadrons (in the present case of charged hadrons that have been measured by ALICE) is included in the unknown function $\mathcal{F}(\tau)$.

Expression (10) will be used in the following to look for GS in the multiplicity distributions. Let us, however, note that GS is, in fact, a property of Eq. (7) and that the multiplicity scaling (10) is based on (9), which is not so obvious for the scattering of small systems, like pp.

To integrate (10) over $d^2p_{\rm T}$ we have to change variables

$$p_{\rm T} = \bar{Q}_{\rm s}(W)\tau^{1/(2+\lambda)}, \tag{11}$$

where the *average* saturation scale is defined as

$$\bar{Q}_{\rm s}(W) = Q_0\left(\frac{\xi W}{Q_0}\right)^{\lambda/(2+\lambda)}. \tag{12}$$

Note that the effective power describing the rise of the average saturation scale with energy $\lambda_{\rm eff} = \lambda/(2+\lambda)$ is slightly smaller than $\lambda/2$. Then

$$p_{\rm T}dp_{\rm T} = \frac{1}{2+\lambda}\bar{Q}_{\rm s}^2(W)\tau^{2/(2+\lambda)}\frac{d\tau}{\tau}. \tag{13}$$

Hence

$$\frac{dN_{\rm ch}}{dy} = \left[\frac{1}{2+\lambda}\int\mathcal{F}(\tau)\tau^{2/(2+\lambda)}\frac{d\tau}{\tau}\right]\times S_\perp\bar{Q}_{\rm s}^2(W) = b\times S_\perp\bar{Q}_{\rm s}^2(W). \tag{14}$$

Here b is an energy independent constant related to the integral of $\mathcal{F}(\tau)$ that formally extends up to some maximal τ related to the maximal allowed transverse momentum. Given the fact that—as we shall see below—function $\mathcal{F}$ vanishes rather fast for large τ, the integral in Eq. (14) can be extended to infinity. This issue has been discussed in detail in Ref. [27].

Equation (14) is often used as a definition of the saturation scale (with $N_{\rm ch}$ replaced by $N_{\rm gluons}$) understood as the gluon number density per transverse area.

III. GEOMETRICAL SCALING OF ALICE DATA

In this section we check whether ALICE data [12] on inelastic multiplicity distributions of charged particles exhibit geometrical scaling as well as for what value of λ. We shall show that indeed GS is reached for $\lambda \sim 0.22$–0.24 as it is illustrated in Fig. 1.

To find the best value of λ we have adopted the *method of ratios* described in more detail in Refs. [10]. Let us denote for simplicity

$$N(p_{\rm T}, W) = \frac{1}{2\pi p_{\rm T}} \frac{d^2 N_{\rm ch}}{dy dp_{\rm T}}\bigg|_W . \tag{15}$$

We form ratios of spectra expressed in terms of the scaling variable τ rather than in terms of $p_{\rm T}$,

$$R_{W/W'}(\tau) = \frac{N(\tau, W)}{N(\tau, W')}, \tag{16}$$

and request that $R \sim 1$ over the largest possible interval of τ. Note that this method is sensitive only to the value of λ and not to the actual values of parameters Q_0 and x_0 In the present case we choose 7 TeV for W and $W_1 = 2.76$ or $W_2 = 0.9$ TeV for W'. Therefore we can form two such ratios, which are depicted in Fig. 2 for $\lambda = 0$ (i.e., for $\sqrt{\tau} = p_{\rm T}$) and for $\lambda = 0.24$. We see that, indeed, these two ratios that rise rather steeply with $p_{\rm T}$ remain flat and close to 1 if plotted in terms of $\sqrt{\tau}$ for $\lambda = 0.24$. We interpret this as a signature of geometrical scaling.

To decide on the best value of exponent λ we need to provide a quantitative criterion measuring the "average distance" of experimental values of $R_{W/W'}$ from unity. To this end we propose the following procedure. Since for λ values relevant for the present analysis the first few R points corresponding to low $p_{\rm T}$ lie above 1 (which is the sign of GS violation in a region when nonperturbative effects are of importance), we pick up the first point for which

$$R_{W/W_{1,2}}(\tau_{\rm start}) - 1 \le \Delta_R(\tau_{\rm start}).$$

Here Δ_R is an experimental error of R. For points with $\tau > \tau_{\rm start}$, either ratio R is close to 1 within the experimental errors or it is falling below 1 exceeding Δ_R. Next, since for large transverse momenta $p_{\rm T}$ spectra are getting harder with increasing energy, the values of R start to increase with τ, getting again larger than 1. This is easily visible in Fig. 3 where the vertical scale has been magnified with respect to Fig. 2 for better resolution.

Starting from $\tau_{\rm start}$ that, of course, depends on energy $W_{1,2}$, we compute mean square deviation for given λ,

$$\delta^2_{W_{1,2}}(\lambda) = \frac{1}{n_{W_{1,2}}(\lambda)} \sum_{\tau_n=\tau_{\rm start}}^{\tau_{\rm end}} \frac{(R(\tau_n, W_{1,2}) - 1)^2}{\Delta^2_R(\tau_n, W_{1,2})}, \tag{17}$$

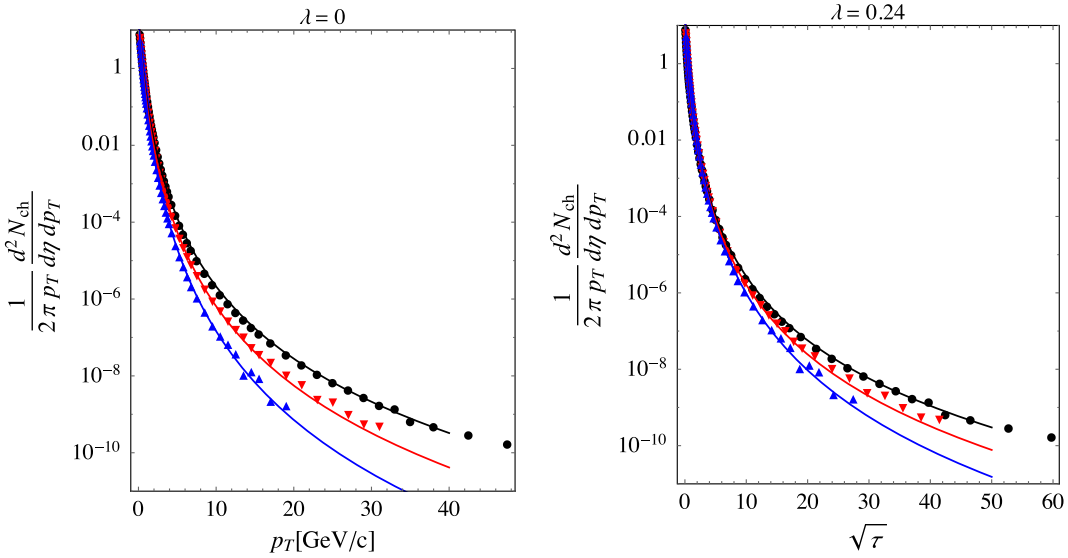

FIG. 1 (color online). Charged particle spectra measured by ALICE [12], plotted as functions of $p_{\rm T}$ (left panel) and as functions of the scaling variable τ (8) for $\lambda = 0.24$ (right panel). Black full dots correspond to $W = 7$ TeV, red down triangles to 2.76 TeV, and blue up triangles to 0.9 TeV. Solid lines correspond to the Tsallis fits from Sec. V.

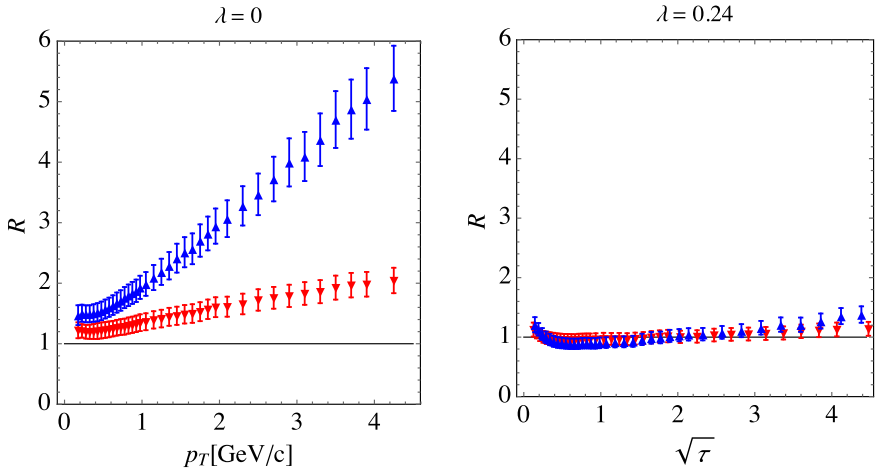

FIG. 2 (color online). Ratios of charged particle spectra measured by ALICE [12], plotted as functions of p_{T} (left panel) and as functions of the scaling variable τ (8) for $\lambda = 0.24$ (right panel). Red down triangles correspond to the ratio $7/2.76$ TeV and blue up triangles to $7/0.9$ TeV.

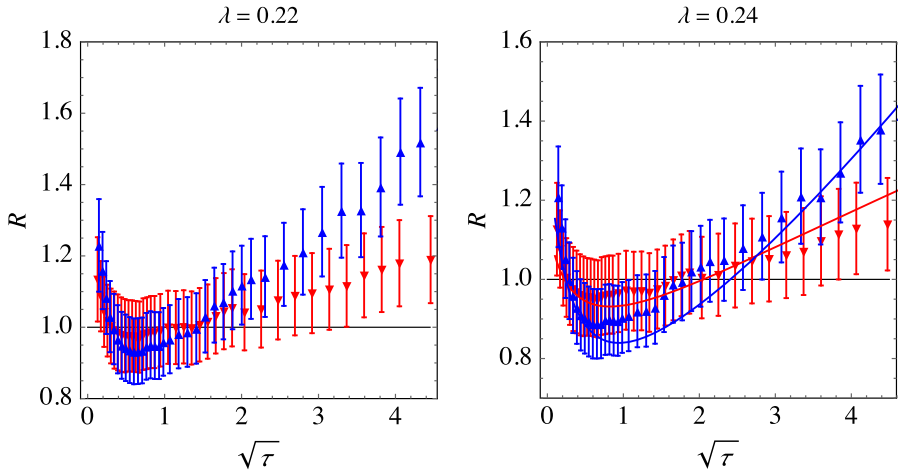

FIG. 3 (color online). Same as Fig. 2 with a different scale for better resolution. Solid lines in the right panel correspond to the Tsallis fits from Sec. V.

where $n_{W_{1,2}}(\lambda)$ is the number of points between τ_{start} and τ_{end}. We increase τ_{end} up to the last point where $\delta^2_{W_{1,2}}(\lambda) < 1$. In this way we obtain $n_{W'}(\lambda)$ which is the number of points that exhibit GS for given $W' = W_{1,2}$ and for given λ, which are plotted in Fig. 4. Now we look for the maximum of $n_{W_1}(\lambda) + n_{W_2}(\lambda)$. This happens for $\lambda = 0.24$. As seen from Fig. 3 $W_2 = 0.9$ TeV points scale in a shorter interval of τ, which translated back to transverse momenta corresponds to $p_{\mathrm{T}}^{\max} = 3.1$ GeV$/c$. We see from Fig. 3 (right panel) that although $\delta^2_{W_2} < 1$, there are 0.9 TeV points (blue up triangles) in the region $\tau_{\mathrm{start}} \le \tau \le \tau_{\mathrm{end}}$ that are below 1 outside the experimental error. If we demand that all points between τ_{start} and τ_{end} should be equal to unity within experimental errors, then $\lambda = 0.22$. This is the value of λ used in Refs. [27] and the relevant plot is shown in the left panel of Fig. 3. The corresponding $p_{\mathrm{T}}^{\max}$ is shifted down to 2.9 GeV$/c$.

Interestingly, when we repeat this procedure for the cross sections that are obtained by multiplying the multiplicity spectra by the minimum bias cross section $\sigma_{\mathrm{MB}}(W)$ given explicitly in Ref. [12], we find that GS occurs at a higher value of $\lambda = 0.31$–0.33. This by itself is not surprising since $\sigma_{\mathrm{MB}}(W)$ depends on energy, and this dependence makes λ different than in the case of multiplicity. What is, however, surprising and encouraging is that the value of λ is now consistent with DIS. Moreover, the range of GS is now larger, up to $p_{\mathrm{T}}^{\max} = 4.25$ GeV$/c$. This is depicted in Fig. 5. The explanation of this observation is beyond the scope of the present paper; however, it is clear that it requires a more sophisticated model of $S_\perp$ of Eq. (9), which in the present analysis is assumed to be an energy independent constant in the case of multiplicity scaling or minimum bias cross section in the case of cross-section scaling.

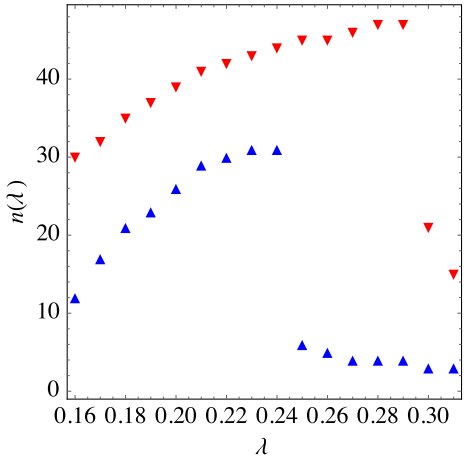

FIG. 4 (color online). Number of points that contribute to (17) for two different ratios: 7/2.76 TeV (red down triangles) and 7/0.9 TeV (blue up triangles) plotted as functions of λ.

We have performed a similar analysis for the UA1 data [28] for the $p\bar{p}$ cross section at $\sqrt{s} = 0.2$, 0.5, and 0.9 TeV with a similar result that $\lambda \approx 0.34$. Here, however, the data extend only up to ~7 GeV/c (for two lower energies) and the tail is quite noisy; namely, the ratios of the cross sections fluctuate quite significantly for $\sqrt{\tau} > 3$.

IV. GEOMETRICAL SCALING AND TSALLIS PARAMETRIZATION

It is well known that particle spectra at low and medium transverse momenta can be described by thermal distributions in transverse mass $m_T = \sqrt{p_T^2 + m^2}$ with "temperature" T, which is a function of the scattering energy [29]. It is also known that more accurate fits are obtained by means of Tsallis-like parametrization [13] where particle multiplicity distribution takes the following form (see, e.g., [30]):

$$\frac{1}{2\pi p_T}\frac{d^2N_{ch}}{dydp_T} = \frac{dN_{ch}}{dy}\frac{p}{E}\frac{C_n}{2\pi}\left[1+\frac{\tilde{E}_T}{nT}\right]^{-n}, \tag{18}$$

where $\tilde{E}_T = \sqrt{m^2 + p_T^2} - m$. In what follows we shall keep $m = 0$, which implies $p/E = 1$. Here

$$C_n = \frac{(n-1)(n-2)}{n^2T^2}. \tag{19}$$

Coefficient C_n in Eq. (19) ensures proper normalization of (18). Indeed,

$$\frac{dN_{ch}}{dy} = \int \frac{1}{2\pi p_T}\frac{d^2N_{ch}}{dydp_T}d^2p_T = \frac{dN_{ch}}{dy}C_n\int_0^\infty dp_T p_T\left[1+\frac{p_T}{nT}\right]^{-n}, \tag{20}$$

where the last integral is equal to $1/C_n$. Here n and T are free fit parameters that depend on particle species and on energy.

In the limit $n \to \infty$ (or equivalently for small p_T) distribution (18) tends to the exponent

$$\frac{1}{p_T}\frac{d^2N_{ch}}{dydp_T} \simeq \frac{dN_{ch}}{dy}\frac{1}{T^2}\exp(-p_T/T). \tag{21}$$

Substituting (11) into (21) we arrive at

$$\frac{1}{p_T}\frac{d^2N_{ch}}{dydp_T} \simeq \frac{dN_{ch}}{dy}\frac{1}{T^2(W)}\exp\left(-\frac{\bar{Q}_s(W)}{T(W)}\tau^{1/(2+\lambda)}\right). \tag{22}$$

Equation (22) exhibits geometrical scaling exactly, only when [31]

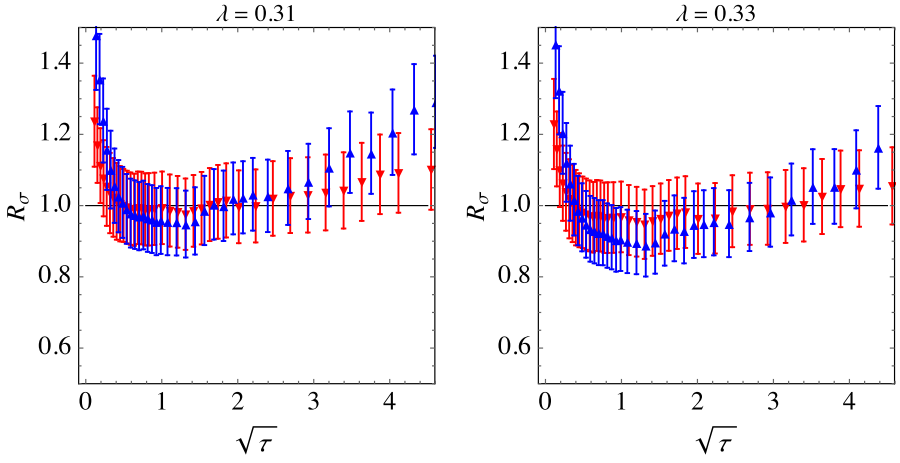

FIG. 5 (color online). Ratios of charged particle cross sections measured by ALICE, plotted as functions of the scaling variable τ (8) for $\lambda = 0.31$ (left panel) and for $\lambda = 0.33$ (right panel). Red down triangles correspond to the ratio 7/2.76 TeV and blue up triangles to 7/0.9 TeV.

$$T(W) = \frac{1}{\varkappa}\bar{Q}_s(W), \tag{23}$$

where $1/\varkappa$ is a constant that should not depend on energy. Then, using Eq. (14), we get

$$\frac{1}{p_T}\frac{d^2N_{ch}}{dydp_T} \simeq \frac{b\varkappa^2}{Q_0^2}\exp\left(-\varkappa\tau^{1/(2+\lambda)}\right). \tag{24}$$

Indeed, (24) is energy independent. This would generalize to the full Tsallis distribution if exponent n were constant. We know, however, from the phenomenological fits that n is decreasing with energy making p_T spectra harder and—in the same time—introducing explicit violation of geometrical scaling for particle spectra.

Let us observe that we can include factor ξ into a definition of b and $\varkappa$, so without any loss of generality we can set $\xi = 1$. Therefore we finally arrive at the GS-Tsallis parametrization of the p_T spectra that reads

$$\left.\frac{1}{2\pi p_T}\frac{d^2N_{ch}}{dydp_T}\right|_W = \frac{B}{Q_0^2}C_{n_W}\left[1+\frac{\varkappa p_T}{n_W\bar{Q}_s(W)}\right]^{-n_W}, \tag{25}$$

where we have introduced new constant $B = b\varkappa^2/2\pi$ and explicitly indicated that n is a function of W. This dependence would be, of course, a source of GS violation. Constants B, $\varkappa$, and Q_0 should remain energy independent.

V. TSALLIS PARAMETRIZATION OF ALICE DATA

In this section we check whether one can fit ALICE data [12] with the help of formula (25). In the original ALICE paper [12] it is said that the multiplicity data can be fitted with the Hagedorn distribution [29], rather than with the Tsallis one. Therefore we could expect that ordinary fitting procedures would not give a reasonable parametrization of the data. To enforce Tsallis parametrization we have proceeded in the following way. For each LHC energy we have chosen two values of p_T, one in the small p_T region and one in the tail that are displayed in Table I. For p_T^{low} we have chosen approximately 0.5 GeV/c that is already above the nonperturbative region. For p_T^{high} we have chosen values that are rather far from the end of the spectrum, but already large enough to be in the perturbative regime. Of course, our fit parameters do depend on this choice; however, as we shall see below, the quality of the Tsallis fits with the values of limiting p_T given in Table I is good enough that manipulating with these values has not been necessary. Let us also remark at this point that our aim here was to show certain properties of the Tsallis fits enforced on ALICE data at low and moderate transverse momenta, since we knew from the beginning that this particular piece of data does not admit Tsallis parametrization in the whole p_T range.

TABLE I. Values of p_T^{low} and p_T^{high} used to fit Tsallis parametrization to ALICE data (see the beginning of Sec. V).

W [TeV]	p_T^{low} [GeV/c]	p_T^{high} [GeV/c]
0.90	0.525	8.5
2.76	0.525	10.5
7.00	0.525	13.5

For the p_T values given in Table I we have calculated ratios $N(p_T^{low}, W)/N(p_T^{high}, W)$, both for the data and for parametrization (25). In this way normalization parameter B canceled out. Now, for a fixed value of $\varkappa$ we have calculated n_W from the following condition:

$$\varkappa: \left.\frac{N(p_T^{low}, W)}{N(p_T^{high}, W)}\right|_{th} = \left.\frac{N(p_T^{low}, W)}{N(p_T^{high}, W)}\right|_{exp} \Rightarrow n_W. \tag{26}$$

Note that the value of parameter λ entering the definition of the saturation scale (12) has been already fixed by the method described in Sec. III. Here we have used $\lambda = 0.24$.

Next, for each pair $(\varkappa, n_W)$ we have computed mean quadratic deviation

$$\sigma_W^2(\varkappa) = \frac{1}{i_{max}^W}\sum_{i=1}^{i_{max}^W}\frac{(N(p_T^i, W)|_{th} - N(p_T^i, W)|_{exp})^2}{\Delta^2(p_T^i, W)}, \tag{27}$$

where i runs over experimental data points at energy W up to the maximal p_T. Δ denotes the experimental error of N. The result is plotted in Fig. 6. We see that functions $\sigma_W^2(\varkappa)$ exhibit minima at three distinct values of parameter $\varkappa$. This is the first signal that one cannot fit ALICE data with Tsallis distributions that correspond to the energy independent parameter $\varkappa$. Therefore we have to allow for energy

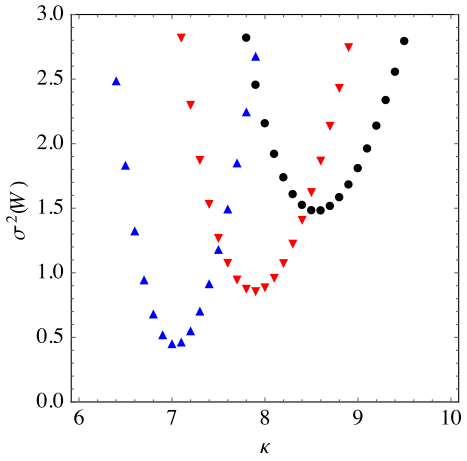

FIG. 6 (color online). Mean square deviations defined in Eq. (27) as functions of $\varkappa$. Black circles correspond to $W = 7$ TeV, red down triangles to 2.76 TeV, and blue up triangles to 0.9 TeV.

TABLE II. Parameters entering Tsallis parametrization (25) coming from the fit to ALICE spectra and the corresponding values of mean square deviation for all measured p_T values and for $p_T < 20$ GeV/c.

W [TeV]	$\varkappa_W$	n_W	B_W	σ_W^2 All p_T	σ_W^2 $p_T < 20$ GeV/c
0.90	7.0	8.32	28.88	0.46	0.46
2.76	7.9	7.33	36.96	0.87	0.71
7.00	8.6	6.79	43.82	1.49	0.75

dependent $\varkappa \to \varkappa_W$, which takes us away from the geometrically scaling Tsallis parametrization of Eq. (25).

One can also see that minima of σ_W^2 grow with energy. This is due to the fact that Tsallis distributions used here are not able to describe both the low p_T part and the very high end of the spectrum simultaneously. We have checked that confining the sums in (27) to $p_T^{\max} \sim 20$ GeV/c corresponding to $i_{\max} = 54$ for all energies in question brings down σ_W^2 below 0.8 (see Table II). This means that Tsallis parametrization with energy dependent $\varkappa_W$ used here is able to describe the p_T spectra at small and moderate transverse momenta, i.e., precisely in the region we are interested in.

In Table II we collect values of the parameters $\varkappa_W$, n_W, and B_W at the minima of σ_W^2. B_W is calculated from the condition $N(p_T^{\rm low}, W)|_{\rm th} = N(p_T^{\rm low}, W)|_{\rm exp}$. The resulting spectra together with ALICE data are shown in Fig. 1 for distributions expressed both in terms of p_T and in terms of scaling variable $\sqrt{\tau}$. The quality of this fit can also be appreciated by looking at the right panel of Fig. 3 where the multiplicity ratios are well reproduced without any adjustment of fit parameters.

Given the fact that the saturation momentum scales as a power of energy $\bar{Q}_s(W) = (W/Q_0)^{\lambda_{\rm eff}}$, we have tried to fit the energy dependence of parameters κ_W, n_W, and B_W with the generic form $a_0(W/Q_0)^\alpha$ with the following result:

$$\kappa_W = 7.097(W/Q_0)^{0.1000},$$
$$n_W = 8.199(W/Q_0)^{-0.1005},$$
$$B_W = 29.76(W/Q_0)^{0.2013}. \quad (28)$$

This result is surprisingly in line with the effective exponent of the saturation scale which for $\lambda = 0.24$ reads $\lambda_{\rm eff} = 0.1071$. Note also that $B \sim \kappa^2$ [see definition of B below Eq. (25)], and this dependence is reproduced by the fits of Eqs. (28). Although this energy dependence follows only from the fit to the data, and we do not have any model to explain their values, it is a reasonable assumption to take,

$$\kappa_W = \kappa_0 \frac{\bar{Q}_s(W)}{Q_0},$$
$$n_W = n_0 \frac{Q_0}{\bar{Q}_s(W)},$$
$$B_W = B_0 \frac{\bar{Q}_s^2(W)}{Q_0^2}, \quad (29)$$

where the coefficients κ_0, n_0, and B_0 can be read off from Eq. (28). In what follows we shall drop $Q_0 = 1$ GeV/c, which was included in (29). Therefore we have

$$\left.\frac{d^2N_{\rm ch}}{dyd^2p_T}\right|_W = B_0\bar{Q}_s^2(W)\frac{(n_0 - \bar{Q}_s(W))(n_0 - 2\bar{Q}_s(W))}{n_0^2} \times \left[1 + \frac{\kappa_0}{n_0}\bar{Q}_s^2(W)\tau^{1/(2+\lambda)}\right]^{-n_0/\bar{Q}_s(W)}. \quad (30)$$

For geometrical scaling to be present we need this function to be independent of W, i.e., independent of $\bar{Q}_s(W)$. For the energies in question (from a few hundreds GeV up to a few TeV) $\bar{Q}_s(W)$ changes from 0.9 to 1.5. Therefore the factor involving n_0 is, in fact, close to 1 and the

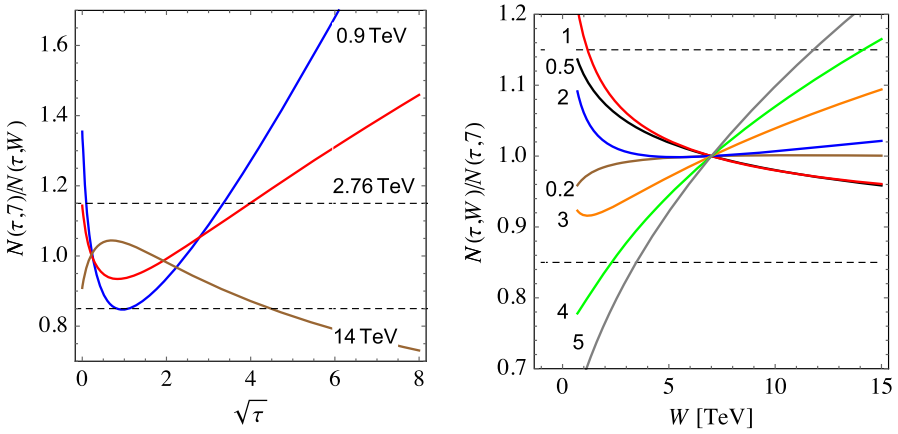

FIG. 7 (color online). Left panel: Ratios (16) in terms of parametrization of Eq. (30) for $W' = 0.9$ (blue curve), 2.76 (red curve), and 14 TeV (brown curve). Right panel: Multiplicities $N(\sqrt{\tau_i}, W)$ normalized to N at 7 TeV plotted as functions of W in TeV for fixed values of $\sqrt{\tau_i}$ displayed next to the vertical axis.

main energy dependence comes from $\bar{Q}_s^2(W)$ in front and from the factor in a square bracket in Eq. (30).

To see how GS is reached by Eq. (30) we plot in Fig. 7 the ratio $N(\sqrt{\tau},7)/N(\sqrt{\tau},W)$ as a function of $\sqrt{\tau}$ for $W = 0.9$, 2.76, and 14 TeV (left panel). Horizontal dashed lines at 1 ± 0.15 show a 15% band around unity, which roughly corresponds to the size of the experimental errors Δ_R (10%) and the accuracy of the fit (5%)—see Fig. 2. GS is present if theoretical solid curves fall within this interval. We can conclude from Fig. 7 that with this accuracy GS should be seen in the data up to $\sqrt{\tau} \sim 4$ for the whole LHC energy range up to 14 TeV. Should Tsallis parametrization (30) hold for higher energies we might expect shrinking of the maximal $\sqrt{\tau}$ where GS is still present with increasing energy. Given the fact that for fixed τ transverse momentum p_T is an increasing function of energy [see Eq. (11)], this may not immediately mean that the p_T window for GS would be shrinking as well.

The same conclusion can be reached by looking at the ratios $N(\sqrt{\tau},W)/N(\sqrt{\tau},7)$ as functions of energy for fixed τ, which are shown in the right panel of Fig. 7 where we plot $N(\sqrt{\tau},W)/N(\sqrt{\tau},7)$ for different values of $\sqrt{\tau} = 0.2$, 0.5, 1, 2, 3, 4, and 5 shown next to the horizontal axis.

VI. CONCLUSIONS

In this paper we have addressed three questions concerning saturation in high energy pp scattering. To this end we have used recent ALICE data on inelastic scattering at the LHC [12].

The first question concerned the very existence of geometrical scaling in multiplicity distributions. By applying a model-independent *method of ratios* we have established that GS is indeed present in multiplicity spectra over a limited transverse momentum range up to ~ 3 GeV/c with characteristic exponent $\lambda \sim 0.22$–0.24. This exponent is significantly different than in DIS, where $\lambda = 0.32$, and also lower than the one extracted from the CMS nonsingle diffractive data: $\lambda = 0.27$. We have proposed the solution to this discrepancy by looking at GS for the inelastic cross section rather than for the multiplicity distribution. Motivation for this comes from the k_T factorized form of the gluon production in pp collisions (4) that leads straightforwardly to Eq. (7) and from the fact that the proportionality factor between the multiplicity and the cross section (9) is not energy independent. We have found that the inelastic cross section scales better than multiplicity up to the maximal transverse momentum that is larger than 4 GeV/c and with the characteristic exponent $\lambda \sim 0.31$–0.33. We have also looked at the UA1 data for $\bar{p}p$ scattering and obtained a similar value of λ. We believe that this observation provides a solution to the discrepancy between scaling properties in DIS and in hadronic collisions.

The second question concerned the universal shape of GS and its connection to the Tsallis distribution. We have confirmed that the natural answer to this question is provided by a parametrization where the Tsallis "temperature" T is proportional to the average saturation scale $\bar{Q}_s$ (12) and the remaining Tsallis parameter n should be an energy independent constant. In practice n does depend on energy, and this leads to the violation of GS for this particular parametrization.

Finally, the third question was whether such a simple solution is admitted by the experimental data. We have found that recent ALICE data on inelastic charged particle multiplicity does not admit the above solution, in agreement with the original claim of Ref. [12]. We have found another parametrization where Tsallis parameter n is inversely proportional to $\bar{Q}_s$. This parametrization indeed exhibits GS in the limited energy range; however, GS is not obviously extended to higher energies. We have concluded at this point that the solution we found was rather accidental. It will therefore be interesting to see whether this solution will still be present at higher energies of the LHC run II.

Obviously neither Tsallis nor thermal distributions have been theoretically derived from first principles or from phenomenological models of hadronic interactions. The fact that particles produced in pp (small system) scattering exhibit thermal distribution has been always regarded as a surprise. Nevertheless present ALICE data show perhaps for the first time strong deviation from these simple parametrizations. Therefore using the analytical form of Eq. (18) may lead to misinterpretations, especially in the context of identifying Tsallis temperature with the saturation scale. This conclusion is further reinforced by our observation that it is a cross section that exhibits better geometrical scaling than multiplicities. Indeed, statistical arguments that may apply to the number of produced particles cannot be simply extended for the cross sections.

Certainly the shape of p_T distribution (and/or of the cross section) can be obtained numerically within models of hadron scattering, and one cannot exclude that no simple and intuitive analytical parametrization exists. Geometrical scaling may continue to exist at asymptotically high energies meaning that parametrization (30) will not work beyond present LHC energies.

ACKNOWLEDGMENTS

This research has been financed in part by the Polish NCN Grant No. 2014/13/B/ST2/02486.

[1] A. H. Mueller, arXiv:hep-ph/0111244.
[2] L. McLerran, Acta Phys. Pol. B **41**, 2799 (2010).
[3] I. Balitsky, Nucl. Phys. **B463**, 99 (1996); Y. V. Kovchegov, Phys. Rev. D **60**, 034008 (1999); Phys. Rev. D **61**, 074018 (2000).
[4] J. Jalilian-Marian, A. Kovner, A. Leonidov, and H. Weigert, Nucl. Phys. **B504**, 415 (1997); Phys. Rev. D **59**, 014014 (1998); E. Iancu, A. Leonidov, and L. D. McLerran, Nucl. Phys. **A692**, 583 (2001); E. Ferreiro, E. Iancu, A. Leonidov, and L. D. McLerran, Nucl. Phys. **A703**, 489 (2002).
[5] S. Munier and R. B. Peschanski, Phys. Rev. Lett. **91**, 232001 (2003); Phys. Rev. D **69**, 034008 (2004).
[6] A. M. Stasto, K. J. Golec-Biernat, and J. Kwiecinski, Phys. Rev. Lett. **86**, 596 (2001).
[7] L. D. McLerran and R. Venugopalan, Phys. Rev. D **49**, 2233 (1994); Phys. Rev. D **49**, 3352 (1994); Phys. Rev. D **50**, 2225 (1994).
[8] Throughout this paper we shall generically denote by $\mathcal{F}$ an energy independent function of scaling variable τ, although in some cases some constant factors are included in $\mathcal{F}$ without changing notation.
[9] L. McLerran and M. Praszalowicz, Acta Phys. Pol. B **41**, 1917 (2010); Acta Phys. Pol. B **42**, 99 (2011).
[10] M. Praszalowicz and T. Stebel, J. High Energy Phys. 03 (2013) 090; J. High Energy Phys. 04 (2013) 169.
[11] M. Praszalowicz, Phys. Rev. D **87**, 071502 (2013).
[12] B. B. Abelev *et al.* (ALICE Collaboration), Eur. Phys. J. C **73**, 2662 (2013).
[13] C. Tsallis, J. Stat. Phys. **52**, 479 (1988); Eur. Phys. J. A **40**, 257 (2009); T. S. Biró, G. Purcsel, and K. Ürmössy, Eur. Phys. J. A **40**, 325 (2009).
[14] C. Y. Wong and G. Wilk, Acta Phys. Pol. B **43**, 2047 (2012); Phys. Rev. D **87**, 114007 (2013); arXiv:1309.7330.
[15] J. Cleymans, G. I. Lykasov, A. S. Parvan, A. S. Sorin, O. V. Teryaev, and D. Worku, Phys. Lett. B **723**, 351 (2013); M. D. Azmi and J. Cleymans, J. Phys. G **41**, 065001 (2014); L. Marques, J. Cleymans, and A. Deppman, Phys. Rev. D **91**, 054025 (2015).
[16] L. J. L. Cirto, C. Tsallis, C. Y. Wong, and G. Wilk, arXiv:1409.3278; C. Y. Wong, G. Wilk, L. J. L. Cirto, and C. Tsallis, EPJ Web Conf. **90**, 04002 (2015).
[17] L. V. Gribov, E. M. Levin, and M. G. Ryskin, Phys. Lett. B **100**, 173 (1981).
[18] Y. V. Kovchegov and K. Tuchin, Phys. Rev. D **65**, 074026 (2002).
[19] A. Szczurek, Acta Phys. Pol. B **35**, 161 (2004).
[20] K. J. Golec-Biernat and M. Wüsthoff, Phys. Rev. D **59**, 014017 (1998); Phys. Rev. D **60**, 114023 (1999).
[21] D. Kharzeev, E. Levin, and M. Nardi, Nucl. Phys. **A730**, 448 (2004); **A743**, 329 (2004); **A747**, 609 (2005).
[22] E. Iancu, K. Itakura, and S. Munier, Phys. Lett. B **590**, 199 (2004).
[23] H. Kowalski and D. Teaney, Phys. Rev. D **68**, 114005 (2003).
[24] P. Tribedy and R. Venugopalan, Nucl. Phys. **A850**, 136 (2011); Nucl. Phys. **A859**, 185 (2011).
[25] E. Levin and A. H. Rezaeian, Phys. Rev. D **83**, 114001 (2011).
[26] Ya. I. Azimov, Yu. L. Dokshitzer, V. A. Khoze, and S. I. Troian, Z. Phys. C **27**, 65 (1985); Yu. L. Dokshitzer, V. A. Khoze, and S. I. Troyan, J. Phys. G **17**, 1585 (1991); V. A. Khoze and W. Ochs, Int. J. Mod. Phys. A **12**, 2949 (1997); S. Lupia and W. Ochs, Phys. Lett. B **418**, 214 (1998).
[27] L. McLerran and M. Praszalowicz, Phys. Lett. B **741**, 246 (2015); M. Praszalowicz, AIP Conf. Proc. **1654**, 080001 (2015).
[28] C. Albajar *et al.* (UA1 Collaboration), Nucl. Phys. **B335**, 261 (1990).
[29] R. Hagedorn, Nuovo Cimento Suppl. **3**, 147 (1965).
[30] S. Chatrchyan *et al.* (CMS Collaboration), Eur. Phys. J. C **72**, 2164 (2012).
[31] M. Praszalowicz, Phys. Lett. B **727**, 461 (2013).